High Current Cathode Thermal Behavior, Part II: Experiments

J. E. Polk*, K. D. Goodfellow†
Jet Propulsion Laboratory
California Institute of Technology
Pasadena, California

Abstract

Temperature profiles have been measured along the axis of a thoriated tungsten rod cathode in an argon gas discharge at two ambient pressure levels and current levels ranging from 600 to 1400 A. At an argon pressure of 2800 Pa, the temperature profile increases monotonically from the base toward the tip. The tip temperature increases with increasing temperature. At an ambient pressure of 1470 Pa, a temperature peak at the tip is accompanied by a plateau or second peak further upstream. With increasing current the magnitude of the upstream peak increases dramatically. Qualitative observations of the arc attachment suggest that at the higher pressure, increases in the discharge current can be accommodated by increases in the cathode tip temperature. At the lower pressure level the tip region can no longer satisfy the current demands and arc attachment further upstream along the cylindrical shaft becomes more important. The decrease in pressure therefore precipitates a transition from a tip attachment mode to a more diffuse cathode attachment. Long thermal transients were also observed at all operating conditions.

Introduction

The service life of thermionic cathodes is important for a number of high current discharge devices, particularly several classes of electric thrusters such as electrothermal arcjets and magnetoplasmadynamic (MPD) engines. Low thrust levels dictate burn times of several thousand hours, and the cathodes of these devices are often the life-limiting component.

Cathodes in high current discharges are subject to several physical processes which cause loss of cathode material and eventual failure.[1]. The most important mechanisms for cathode mass loss include ejection of molten material, evaporation of bulk cathode material and cathode additives, chemical attack by reactive propellant gases or contaminants and sputtering by high velocity ions. With the exception of sputtering, the rates of all of these mechanisms are strongly dependent on the cathode temperature. Assurance of adequate service life therefore requires a quantitative understanding of high current cathode thermal behavior.

Cathodes in arc discharges operate in a number of different modes which can be categorized in two broad groups nonstationary cathode modes in which electrons are released in explosive emission phenomena or thermal-field emission in small regions due to Joule or ion impact heating and stationary modes where the electron current is supplied by field-enhanced thermionic emission [2]. The nonstationary modes occur on relatively cold cathodes which cannot supply the required current by thermionic or field-enhanced thermionic emission. Stationary cathode operation in electric thrusters can be further subdivided into the Low Pressure Thermionic Spot Mode or "diffuse attachment" mode, which occurs on high temperature, low work function cathodes in a low pressure ambient gas, and the High Pressure Thermionic Spot Mode or "tip attachment" mode, which forms on cathodes at higher pressures. Diffuse attachment is usually observed on MPD thruster cathodes where

* Technical Group Leader, Advanced Propulsion Technology Group
† Member of the Technical Staff, Advanced Propulsion Technology Group

the discharge occupies a substantial portion of the cathode surface. Tip attachment occurs 011 cathodes in the higher pressure environment of arcjet discharge chambers and is characterized by a much smaller arc. attachment point in which the temperature may be above the melting point.

A companion paper [3] describes the theoretical understanding of stationary cathode operation in both the tip attachment and diffuse attachment n iodes. A model of the near-cathode plasma is used to define the boundary conditions for a thermal n iodel which yields the cathode temperature. However, there is a limited database of cathode temperature measurements to compare with model predictions and no detailed characteri zations of the near catl - ode plasma. Some temperature measurements have been performed in electric thrusters [4,5,6,7,8,9], but the only systematic study of cathode ther mal behavior was conducted by Hügel and Krülle [10,1 1]. They measured cathode temperature distributions on a rod-shaped thoriated tungsten catl iode at argon, helium and hydrogen pressures ranging from 2000 l'a (15 'J'err) to 13300 Pa (1(10 Torr) and current levels from 200 to 1000 A.

To extend the database of cathode temperature measurements and provide a better characterization of the near-cathode plasma properties which arc important inputs to the model, a dedicated cat hode test facility has been constructed. In this paper the facility and temperature diagnostics will be described and temperature data obtained at currents of 600 to 1400 A and ambient argon pressures of 1470 Pa (11 'J'err) to 2800 Pa (21 'J'err) will be presented.

Experimental Apparatus

The Cathode Test Facility

The cathode test facility is shown in the diagram in Fig. (l). The stainless steel vacuum chamber is 0.5 m in diameter and 2.4 m long and is composed of 4 water-c.oo]ccl cylindrical segments. As the schematic in Fig. (2) shows, the first segment forms the discharge chamber. A Water-cooled, ring-shaped copper anode with a diameter of 7.6 cm is mounted 011 a flange located between and electrically isolated from the first two tank segments. The cathode fixture mounted on the vacuum chamber door is composed of two coaxial tubes electrically isolated from eacl I other and the door with micarta rings. The inner tube serves as the cathode current feed and has a water-cooled cap 011 the end to which the catl - ode is clamped. The outer tube is electrically floating and has a water-cooled copper disk mounted 011 the end with an aperture through which the cathode protrudes. The prop ellant gas is injected between the two tubes and flows into the discharge chamber through an annulus around the base of the cathode. The interelectrode gap is set by the thickness of a spacer in the cathode assembly. The cathode used in this investigation is a rod of 2 percent thoriated tungsten 76111111 long and 9.5 mm in diameter with a hemispherical tip. The last tank segment contains a heatexchanger made of water-cooled, finned copper tubing to cool the exhaust before it enters the pumping system. The tank has a number of ports which provide optical access to the discharge chamber as well as the plum e. In addition, the cathode and the discharge can be viewed along the tank axis through a window at the rear of the tank.

The vacuum chamber is pumped by a 610 1/s Roots blower backed by a 140 l/s Stokes mechanical pump. The system is capable of achieving a vacuum of less than 0.13 Pa (1 IIfl'err) with no propellant flow and ap proximately 80 Pa (0.6 '1'err) with an argon flow rate of 0.75 g/s. Higher ambient gas pressures arc achieved by bleeding ad ditional gas into the chamber through a fitting in the third segment and/or by turning off the Roots blower. The ambient pressure can be controlled to within approximately ±1 7 0 Pa (0.5 Torr). The arc is powered by two Miller welding power supplies, each of which can provide 1500 A at a load voltage of 40 V continuously or 2000 A at 40 V with a 50 percent duty cycle. The initial arc breakdown is accomplished with a 4 A, 850 V start supply.

The factory shunts in the Miller welders have been replaced with precision shunts that are used to monitor the arc current. The Aerminal volt age is measured at the current feedthroughs into the tank. The propellant flow 'rate is measured with a Sierra Instruments Side-'lkak Model 830 flow meter and controlled with a throttling valve located just upstream of the inlet to the cathode fixture. "J 'he flow meter output was calibrated by measuring the mass loss from an argon bottle as a function of time. An MKS Baratron capacitance manometer with a range of 0-

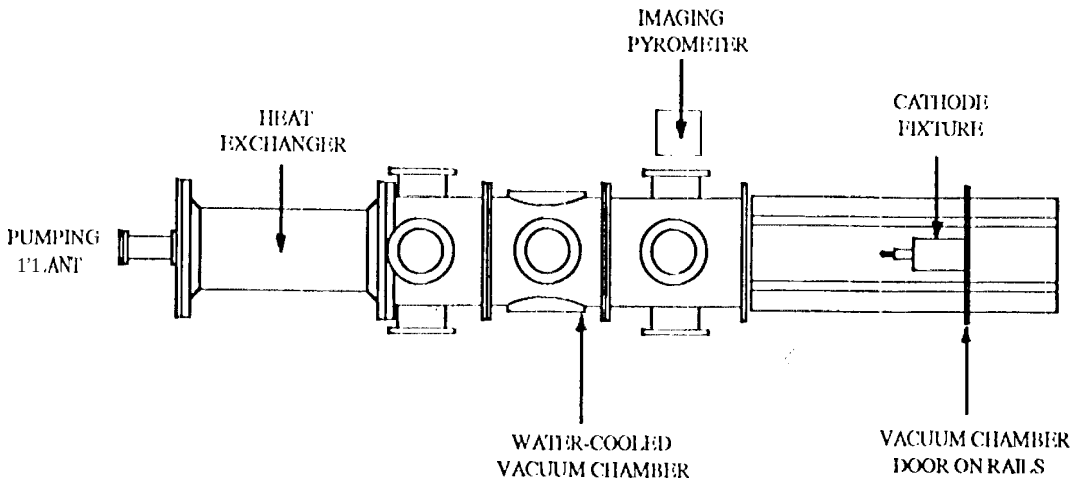

Figure 1: Diagram of the cathode test facility.

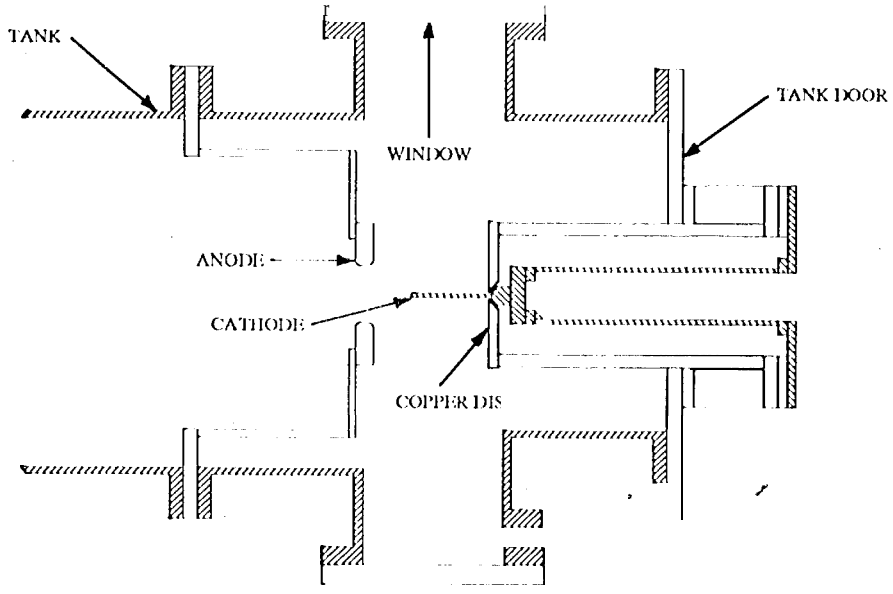

Figure 2: Schematic of the electrode configuration.

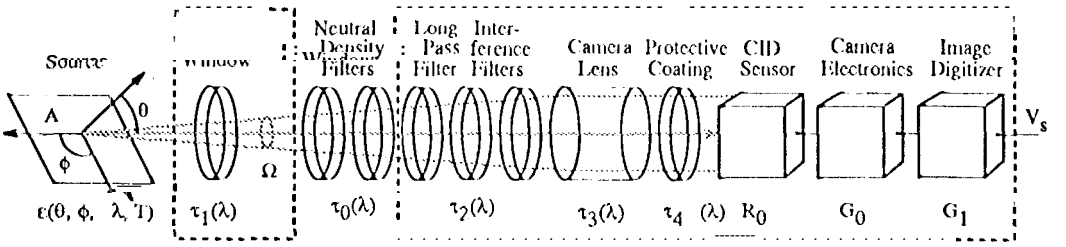

Figure 3: Diagram of imaging pyrometry system.

1.3×10^5 Pa which is mounted 011 the tank door is used to measure the discharge chamber pressure. These parameters and a number of facility temperatures are recorded with a Macintosh computer system utilizing LabView software and National Instruments multi-purpose I/O cards.

The Temperature Measurement System

The Imaging Pyrometer

A CIDTEC 2550-D Charge Injection Device (CID) camera was chosen as an optical pyrometric sensor to measure the two-dimensional temperature field 011 the cathode. Figure (3) shows a diagram of the system. An area A on the source emits a spectral radiance of $\epsilon(\theta, \phi, \lambda, T) L_{b\lambda}(\lambda, T)$, where $\epsilon(\theta, \phi, \lambda, T)$ is the surface emittance at wavelength λ at an angle θ relative to the surface normal and ϕ from some reference line on the surface, and $L_{b\lambda}(\lambda, T)$ is the radiance of a black body at the same temperature T. This area is viewed by the system optics through a window with a transmittance of $\tau_1(\lambda)$ and one or more neutral density filters with a combined transmittance of $\tau_0(\lambda)$. The system optics are composed of two interference filters with a 10 nm bandpass centered at 632.8 nm and a long pass filter with a cutoff wavelength of 570 nm, all three with a combined transmittance $\tau_2(\lambda)$; a normal camera lens with a transmittance $\tau_3(\lambda)$; and a protective coating on the sensor array with a transmittance of $\tau_4(\lambda)$. The optics intercept radiation emitted by the area into a solid angle Ω and focus it onto the CID sensors in the camera array. The detector output V_d for an input power W is defined as the responsivity of the sensor, R_0. The imaging array has 512 x 512 CID detectors which are read out at a maximum rate of thirty times per second. These values are converted to an analog signal, which is then further processed and output as a normal video signal by the camera electronics, which have a gain of G_0. The video signal is digitized by a Data Translation DT-2862 8-bit frame-grabber board with a gain of G_1, which yields a final value between 0 and 255 corresponding to the incident power.

Calibration of the Pyrometer

The system enclosed in dashed lines in Fig. (??), which includes the camera and associated electronics, all optical components except the neutral density filters, and the detector-source geometry, was calibrated as a unit. The neutral density filters are chosen to properly moderate the input radiance and may be varied from experiment to experiment depending 011 the source intensity. Their transmittance is therefore calibrated separately and used to scale the calibration for the subsystem shown inside the dashed lines.

The incident power is given by radiance of the source transmitted by the various intervening media integrated over the spectrum, the emitting area, and the intercepted solid angle,

$$W = \int_0^\infty \int_A \int_\Omega L_{b\lambda}(\lambda, T) \epsilon(\theta, \phi, \lambda, T) \times \prod_{i=0}^{4} \tau_i(\lambda) \cos\theta \, dA \, d\lambda \, d\Omega. \quad (1)$$

The blackbody radiance $L_{b\lambda}$ is described by Planck's spectral radiance distribution:

$$L_{b\lambda} = \frac{2hc^2}{\lambda_{ij}^5} \frac{1}{e^{hc/\lambda_{ij}kT} - 1} \approx \frac{2hc^2}{\lambda_{ij}^5} e^{-hc/\lambda_{ij}kT} \quad (2)$$

where h is Planck's constant, k is Boltzmann's constant, and c is the velocity of light. The second expression is Wien's Law, an approximation that is valid for the temperature range of interest. Assuming that the directional emittance $\epsilon(\theta, \phi, \lambda, T)$ does not vary significantly over the solid angle Ω and that the interference filter blocks sufficiently well in regions outside of a narrow band $\Delta\lambda$ at a central wavelength of λ_{ij}, the integral can be simplified to

$$W = A \cos\theta \, \Omega L_{b\lambda}(T) \epsilon(\theta, \phi, T) \prod_{i=0}^{4} \tau_i \Delta\lambda \,|_{\lambda = \lambda_{ij}} \quad (3)$$

where $A \cos\theta$ is the projected area in the viewing direction. The responsivity R^*, which relates the system output V_s to the source radiance at the interference filter wavelength through the neutral density filters L_λ^*, is defined as

$$R^* = R_0 G_0 G_1 A \cos\theta \, \Omega \prod_{i=1}^{4} \tau_i \Delta\lambda = \frac{V_s}{L_{b\lambda}(T) \epsilon(\theta, \phi, T) \tau_0} = \frac{V_s}{L_\lambda^*}. \quad (4)$$

This is the desired calibration relation which contains the responsivities of the electronic components, the source-detector geometry, and the optical component parameters. If the gains of the electronic components are constant, the system responsivity R^* should have the same functional form as the camera responsivity R_0, which is constant up to a point in the range of 50-80 percent of the saturation value, after which it decreases. Equation (4) also emphasizes that each optical setup and source-detector geometry must be individually calibrated. The value R^* must be empirically determined using a reference source with a known temperature and emittance at the interference filter wavelength, accounting for the transmittances τ_0 of the media between the source and the camera optics. This measured R^* can then be used to determine the temperature of another source with known emittance viewed through filters with known transmittances.

The subsystem responsivity R^* was measured with a Mikron model M300 blackbody calibration source and independently with an Eppley tungsten ribbon **lamp.** The blackbody source had an emissivity of 0.999± 0.005. The temperature of the spherical cavity was measured to within ±1°C with a Type S thermocouple embedded in the wall. The radiance L_λ^* of the source was calculated from the measured temperature using the Planck distribution in Eq. (2) and the emittance. The possible error in the calculated radiance due to uncertainties in the temperature is less than ± 2.5 percent. The source was operated over a temperature range of 900 to 10 85° C, corresponding to a radiance range of 0.44 to 7 mW/μm cm^2 sr.

The aperture of the cavity was imaged on the array with the same detector-sclurce geometry used in the experiments, but with no neutral density filters. The temperature was set and allowed to stabilize to within ± 1°C before measuring the system response. The radiance was uniform only across the right-hand side of the aperture, decreasing slightly on the left. Therefore, only the response of 50-100 pixels illuminated by the uniform part of the image was measured. These measurements were also used Lo determine the intrinsic variability in pixel response. Experiments performed with the source held at a constant temperature over five hours show no drift in pixel output and random fluctuations on the order of ± 2 gray levels, The uncertainty associated with these fluctuations can be reduced to a negligible level by averaging a number of frames.

The radiance in the center portion of the tungsten ribbon lamp was determined by comparison with an Optronics Model 550 calibration lamp traceable to NIST standards using an Optronics Model 746-1) spectroradiometer, and is accurate to within ± 3 percent. The lamp was operated over a radiance range of 0.35 to 6.23 mW/μm cm^2 sr and the center part of the ribbon was imaged on the detector array. The response of 5 pixels illuminated by the uniform part of the image was measured. These data were also used to cst imate the variation in response from pixel to pixel. The variation among the 5 detectors did not exceed 1 gray level up to 150 gray levels and not more than 1 „5 gray levels at saturation)].

Figure (4) shows the final calibration curve relating

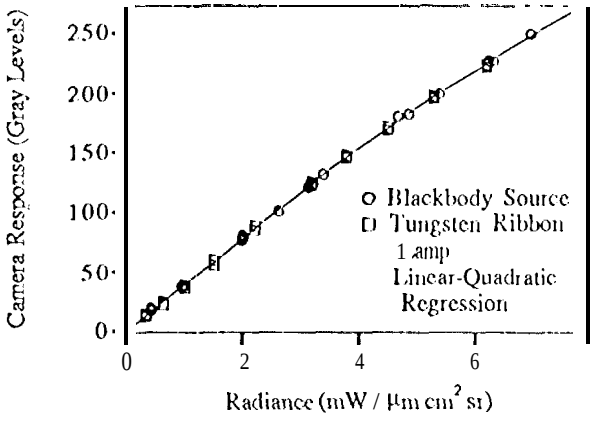

Figure 4: CIDTEC camera calibration.

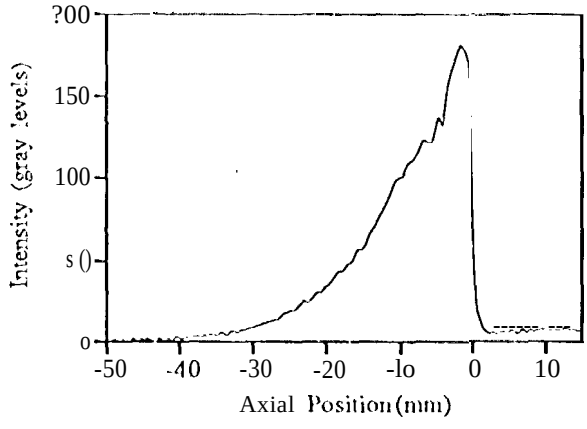

Figure 5: Cathode axial intensity distribut ion.

the camera output V_s to the incident radiance L^*_λ. The slope of this curve is the responsivity defined in Eq. (4) and, as expected, is constant until about gray level 117, then drops off. The data can be well represented by the function

$$V_s = \phi_1 + \phi_2 L^*_\lambda + \phi_3(\alpha - L^*_\lambda)^2_- \qquad (5)$$

where α is the position of the knee, and the subscript minus sign at the end of the last term signals that it is to be included only when L^*_λ is greater than α. The parameters ϕ_1, ϕ_2, ϕ_3, and α were estimated using a non-linear fitting program.

The transmittance of the neutral density filters was measured using a tungsten coil lamp arid the spectroradiometer with an uncertainty of approximately ± 3 percent.

Application in the Experiments

In the experiments the camera and optics were mounted outside the chamber about 39.5 cm from the cathode. The video output from the camera was digitized to provide real-tilllc monitoring of the temperature distribut ion. One line in video memory chosen to correspond to the axis of the cathode was sampled from each frame. A given number of lines were averaged, displayed in real time, and periodically stored on disk. Figure (5) shows a typical cathode axial profile obtained by averaging 20 frames. The axial position is measured in mm from the cathode tip and is defined to be positive in the downstream direction. A small signal due to radiation from the plasma plume is visisble downstream of the cathode. The intensity varies with the pressure and the current level, but is typically 7 to 15 gray levels.

The inverse of the calibration relation given in Eq. (5) was used to determine the radiance incident on the system from the measured response. The temperature is determined from Planck's distribution, Eq. (2), the cathode emittance and neutral density filter transmittance, and the measured radiance,

$$T = \frac{hc}{\lambda_{if} k}\left[\ln\left(\frac{2hc^2}{\lambda_{if}^5}\frac{\epsilon(\theta,\phi,T)\tau_0}{L^*_\lambda} + 1\right)\right]^{-1}. \qquad (6)$$

Uncertainty in the Temperature Measurements

The uncertainty in the temperatu re measurement is given approximately by the expression

$$\frac{\sigma_T^2}{T^2} = \left(\frac{\lambda_{if} kT}{hc}\right)^2\left[\frac{\sigma_\epsilon^2}{\epsilon^2} + \frac{\sigma_{\tau_0}^2}{\tau_0^2} + \frac{\sigma_{L^*_\lambda}^2}{L^{*2}_\lambda} + \left(5 - \frac{hc}{\lambda_{if} kT}\right)^2\frac{\sigma_{\lambda_{if}}^2}{\lambda_{if}^2}\right]. \qquad (7)$$

The sensitivity to the independent parameters is small because the multiplying factor $(\lambda_1 kT/hc)^2$ is approximately equal to 0.01-0.02. The interference filter is assumed to block perfectly outside a narrow region, so the last term is negligible. Uncertainties in the neutral density filter transmittance contribute approximately 1 percent to the standard error. The primary contributors to the uncertainty are the relatively large and, to a certain extent, unquantifiable errors in the emittance of the cathode surface and the proper measurement of the incident radiance.

The emittance of the cathode surface was assumed to be independent of the viewing angles θ and ϕ, which is true for diffuse emitters, and rough surfaces often approach this behavior. In addition, since the cathode axial temperature profiles were taken parallel to the surface normal, measurements for the normal emittance of tungsten were used in the analysis. A curve fit performed by Pon [12] to emittance data for tungsten ribbon lamps measured by DeVos [13] for the wavelength 632.8 nm yields emittances ranging from about 0.44 at 2000 K down to 0.42 at 3400 K. The errors in the measurements and the curve fit are quoted to be about 2 percent. To simplify the analysis an intermediate value of 0.43 corresponding to the emittance at 2800 K was used in Eq. (6) for all temperatures. This approximation represents an error in emittance of about 2.5 percent at 2000 K, but a very small error in the temperature range of interest.

However, this data is not necessarily representative of the cathode surface because emittance is extremely sensitive to surface topology and chemical composition. Roughness can substantially increase the emittance, and limited data from [14] indicate that the emittance for a tungsten surface with a characteristic roughness of 1-3 μm could be as high as 0.6 in the wavelength range of interest. Since the energy radiating from a surface is characteristic of the material in a thin layer less than 1000 Å thick, relatively thin oxide layers can have a significant impact. Because it is virtually impossible to adequately characterize a surface or quantify the effect of surface irregularities and composition, the emittance should ideally be measured in the experiment. Measurements of emittance using cathodes containing small, high-emittance cavities [4,7,15] or unspecified methods [16] are inconclusive. The measured values range from about 0.4 to as high as 0.8.

The uncertainty in the estimate of incident radiance L_λ^* depends on three factors - the uncertainty in the system output determination, uncertainties arising from the calibration curve fit, and systematic errors associated with inapplicability of the calibration relation. As discussed above, the variation in sensor output can be reduced below one gray level by averaging a sufficient number of measurements. In all analyses 20 samples were averaged, giving a random error in the determination of V_s under the inherent digitizer resolution, less than 0.5 percent. The uncertainty in the fit, which reflects the random errors in the calibration measurements, is on the order of 0.04 1111$'///111 cm^2, or less than 0.5 percent at the higher temperatures. However, there could be a systematic error in the calibration equal to the uncertainty in the radiance values of the calibration sources, which is about 3 percent.

The applicability of the calibration rests on the validity of the assumptions leading to Eq. (4). It is assumed that the gains of the electronic components are constant, and that the detector responsivity R_0 is the same for all sensors in the array, because the sensors which receive the cathode image in the experiments are not necessarily those used in the system calibration. The tests with the blackbody source indicated that there is very little drift in the system gain. In addition, the variability among image pixel outputs is only 0.5 to 1.5 gray levels, and the effect of this uncertainty on temperature measurements can be minimized by averaging several adjacent pixels.

The calibration relation also contains the source-detector geometry in the terms $A \cos\theta\, \Omega$, so errors in these factors produce an uncertainty in the calculated radiance. For the focal length and source-detector distance used in these tests an error in the setup distance of as much as 25111111 produces less than a 1 percent deviation from the responsivity measured in the calibration.

For the calibration relation (o be valid the system optics must have the same transmittances as those used for the calibration. This requires that the same optics be used, that the surfaces be kept clean, and that all adjustable aperture settings be repeatable. The maximum aperture of the lens was chosen because intermediate settings of the diaphram proved to be irreproduceable. Illumination levels were controlled with neutral density filters.

The final assumption used in the calibration is that the observed radiance is emitted by the cathode surface, and not other sources such as plasma radiation. The interference filter was chosen because it minimized the contribution from the intense plasma. The prime contributor is apparently continuum radiation at the wavelength of the interference filters. The plume intensity typically observed several mm in front of the cathode tip corresponds to a bias of only about 20 K, assuming that it is representative of the plasma signal intensity over the cathode surface. Because the plasma layer over the cathode surface imaged by the camera is thinner than the jet in front of the tip, the effect may be even less significant.

In conclusion, random errors in the temperature calculation associated with uncertainties in the transmittance of the neutral density filters, emittance of the surface and the measurement of the incident radiance are well under 1 percent. Systematic errors arising from variations in source-detector geometry and optical parameters can be minimized by careful attention to the experimental set up. However, underestimation of the true emittance because of the effects of roughness or oxide layers can lead to errors as high as 9 percent and plasma radiation perhaps as high as 1 percent. These two effects are difficult to quantify, but both yield an overestimate of the temperature.

Experimental Results

Cathode axial temperature distributions were measured as a function of time at current levels ranging from 600 to 1400 A and an argon mass flow rate of 0.75 g/s for two discharge chamber pressure levels, 2800 Pa (21 Torr) and 1470 Pa (11 Torr). A 1 to 2 A arc was initiated briefly with the high voltage start supply at the desired ambient pressure before the Miller welder supplies were engaged at a preset current level at or near the desired value. After start-up, the cathode experiences a rapid transient associated with cold cathode emission processes and then a slower thermal transient.

The cathode initially operates in the non stationary, cold cathode mode identified by highly mobile, discrete emission sites. After a period of 1 to several seconds, depending on the current level [17], the cathode becomes sufficiently hot to maintain thermionic emission and a transition to a more stationary attachment at the cathode tip occurs. As shown in the photograph in Fig. (6), some portion of the tip and shaft of the cathode is enveloped in a bright, teardrop-shaped plasma plume. This blue inner core is surrounded by a less intense yellow plume that extends from the cathode attachment to the anode.

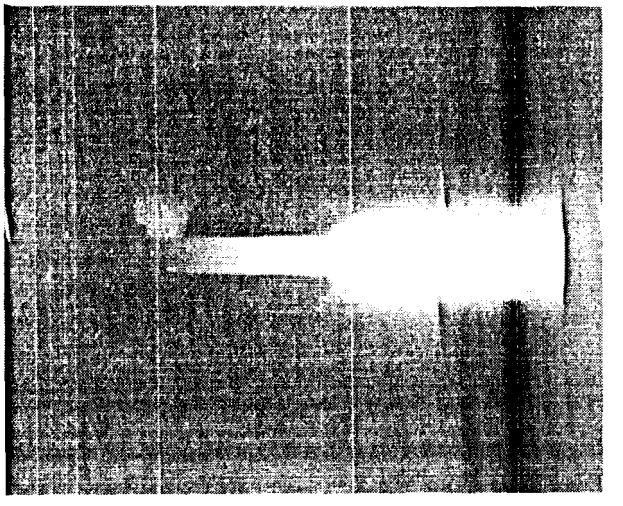

Figure 6: Photograph of the discharge region.

In these experiments the discharge was operated at constant current and pressure conditions for periods ranging from 7 to 90 minutes. In most cases the operating time was sufficiently long for the cathode temperature distribution to reach a stationary state. The cathode thermal behavior as a function of current level and ambient pressure will first be presented, then the transient thermal behavior will be discussed briefly.

Stationary Temperature Distributions

The temperature as a function of axial distance from the tip (positive downstream) measured at 2800 Pa is displayed in Fig. (7). The temperature decreases monotonically from the tip toward the base for all currents tested. The profiles have a characteristic shape, with a a short region at the tip where the temperature is relatively constant, followed by a sharp temperature gradient and then a linear decrease in temperature over most of the upstream part of the shaft. The tip temperature increases slightly with

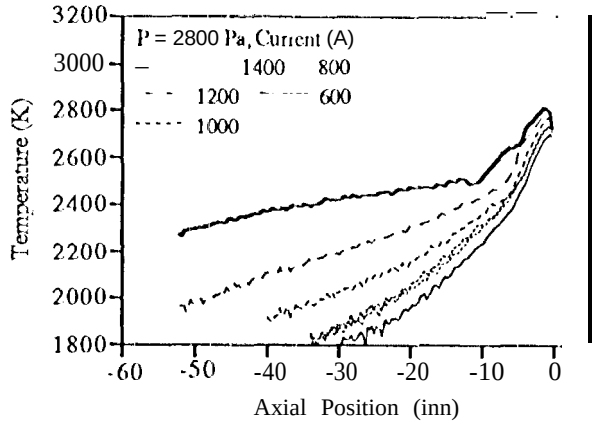

Figure 7: Axial temperature profiles n ieasure at 2800 Pa.

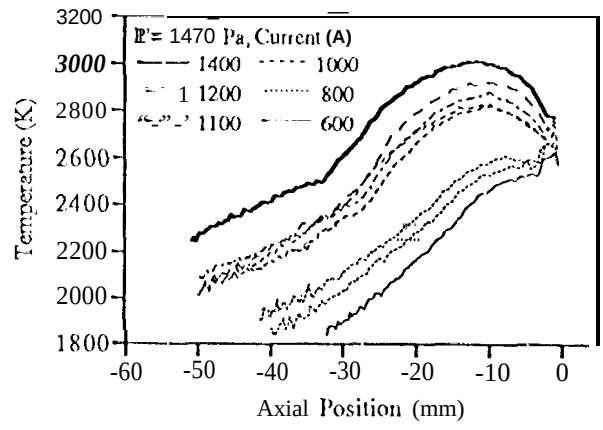

Figure 8: Axial temperature profiles measure at 1470 Pa

current, ranging from about 2700 to 2800 K. The Last temperature increases more rapidly with rising current, producing a flat ter profile. During the experiments at 2800 Pa, the blue plasma plume was confined to the hemispherical tip of the cathode, and the region of fairly uniform temperature corresponded to the part of the cathode enveloped by the plume. Repeatability of these measurements is good, as indicated by the agreement between the two profiles measured at 800 A.

The corresponding temperature profiles measured at a lower pressure of 1470 Pa arc shown in Fig. (8). The characteristic shape of these profiles is considerably different from that observed at the higher pressure. **A** small temperature peak at the tip is followed by either a plateau in temperature or a second peak located further upstream. At this pressure, the tip temperature also rises slightly with cu]-rent, varying over a relatively small range of ?600 to 2800 K. The base ter nperature and the tempera ture along the cathode shaft rise much more dramatically with current. **In** these tests the app earance of the plume was also different from the higher pressure experiments. At low currents, the brightest part of the blue plu me was concentrated on the tip, but a less intense blue plasma covered a portion of the cylindrical shaft upstream of the hemispherical tip. At, higher current levels, the intense blue plume enveloped all of the tip and part of the shaft. Observations of the discharge through a narrow bandpass filter centered at 488 nm, where a strong argon ion line is located, revealed a peak in the intensity in a thin layer less than 1 mm thick near the cathode surface. The brightness of this layer seemed to be highest at the cathode tip and at a location further upstream on the cathode. Comparison of the two measurements made at 1000 **A** and 800 **A** shows that the tip temperature is very repeatable, but that the upstream portion of the profile has some variability.

The temperature variation with current is summarized in Fig. (9). **As** indicated by the individual temperature profiles, the tip ten perature increases with current for both cases, but for a given current level the tip temperature is slightly higher at the higher pressure. For both pressure levels, the rate of tip temperature increase drops with increasing pressure. At the lower pressure, the temperature in the upstream peak is below the tip temperature for low currents, but rises more rapidly and exceeds the tip temperature at a current level between 800 and 1000 **A.**

Temperature profiles measured at 1470 and 2800 Pa for a discharge current of 1000 **A** arc compared in Fig. (10). The tip temperatures arc similar and both curves appear to approach a comparable base temperature, but the behaviors in the middle of the cathode are quite different. The high temperature

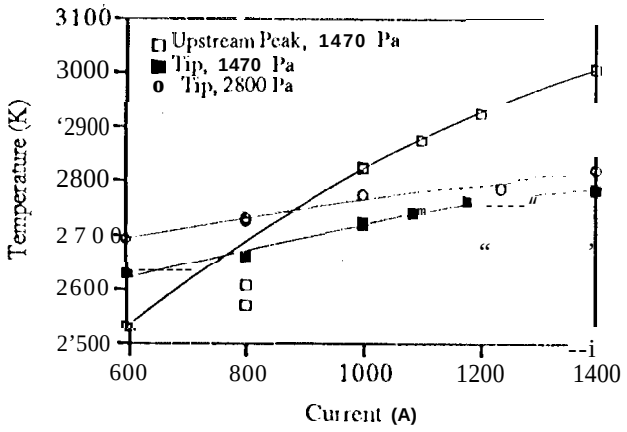

Figure 9: Variation of peak cathode temperatures with current.

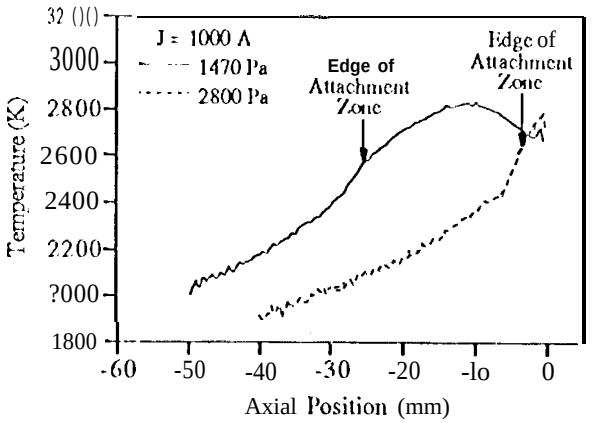

Figure 10: Comparison of temperature profiles at low and high pressures.

region extends much further back in the low pressure case. The upstream boundary of the attachment zone is identified as the knee in the temperature profile, as shown in Fig. (10). The change in slope at this point indicates the end of the region where the high temperature is sustained by heat inputs from the arc attachment. The variation in the location of this boundary and the upstream temperature peak with current is displayed in Fig. (11). At the higher pressure, there is not much change in the length of the attachment zone as the current is increased. However, at the lower pressure the length of the arc attachment region and the location of the temperature peak both increase up to about 1000 A and then become approximately constant.

Transient Thermal Behavior

In all of the experiments the cathode temperature rose over the course of several minutes, asymptotically approaching a stationary distribution. The time constant of these transients generally ranged from 5 to 15 minutes. Figure (12) shows a typical thermal transient for a run at 800 A and 1470 Pa. The tip and the location of the upstream temperature peak start 60 and 20 K lower than their stationary values and approach these values with time constants of about 8 and 12 minutes, respectively. For this case the edge of the attachment zone corresponds approximately to the 2400 K isotherm. The plot of temperature contours for this run in Fig. (13) shows that the length of the attachment region grows with time also, a phenomenon observed in all of the low pressure runs.

Discussion

The behavior observed in these experiments suggests that a transition between tip attachment and diffuse mode attachment triggered by a decrease in pressure is occurring. At a pressure of 2800 Pa, the arc attachment is concentrated on the cathode tip and increases in the total current arc accommodated by increases in the tip temperature. A cathode tip attachment thermal model combined with a model of the near-cathode plasma described in [3] predicts a restricted range of allowable tip temperatures for a given combination of pressure, work function, current level, electron temperature and sheath voltage. For pressure and current values similar to those encountered in these experiments, a work function of about 3.5 eV, an electron temperature of 1 eV and sheath voltages on the order of 10 V a temperature range of about 2600 to 2800 K is predicted, which is consistent with the experimental observations (see Figures (12) and *(13)* in [3]). However, detailed comparisons between the experimental and theoretical behavior have not yet been conducted.

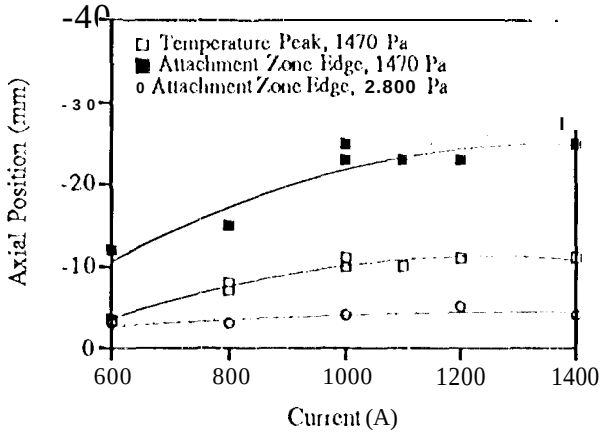

Figure 11: Variation in the position of he attachment zone boundary and the upstream temperature peak with current.

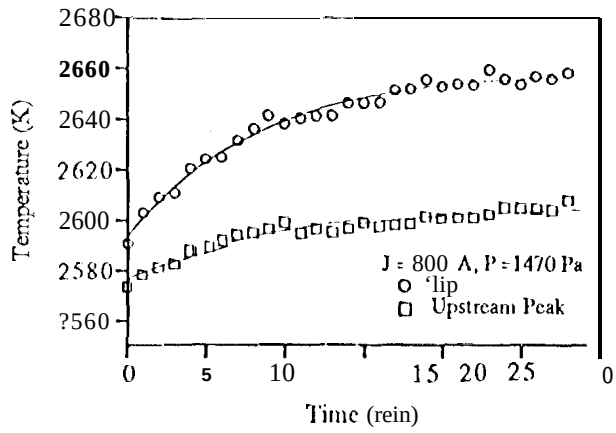

Figure 12: Cathode thermal transient behavior.

At lower pressure levels, the tip region is apparently unable to satisfy all of the current demands. The measured temperature peak at the tip and the observations of the plume intensity in that region indicate that the tip still plays an important role. However, arc. attachment from the cylindrical shaft becomes more importan it and dominates at high current levels. This behavior was also seen by Krülle at low pressures in argon [10], and there is evidence that the temperature peak shifts even further upstream at lower pressures [4,7]. The cathode thermal model cannot yet reproduce the tip temperature peak and the second peak upstream under these conditions. The model tends to predict a temperature profile that is nearly uniform within the region where arc attachment is permitted, with only a slight upstream peak due to Joule heating. This may be an artifact of specifying uniform plasma and surface properties along the cathode axis. The observations with the 488 nm filter suggest that there arc axial variations in the near-c athode plasma within the attachment zone.

The observed thermal transients are not yet understood. The time constants appear to be g;l-cater than those associated with heat conduction through the tungsten. The increase in radiance may be an effect of changing surface conditions. As the surface chemical state or morphology changes, the emittance or the work function may change. This could produce either a true temperature transient or an apparent change in temperature caused by an emittance change.

Subsequent experimental activities will be directed at extending the thermal characterization to both higher and lower pressures, and measuring key model parameters directly. The model will be used to map out the input parameter space to compare with the observations.

Acknowledgements

The research described in this paper was conducted at the Jet Propulsion Laboratory, California Institute of Technology, under a contract with the National Aeronautics and Space Administration.

The authors would like to thank W.R. Thogmartin, R.L. Toomath and A. G. Owens for their technical assistance and dedication in constructing the cathode test facility. The assistance of M. Cerezo in the JPL Standards Laboratory in calibrating the imaging p - rometer is gratefully acknowledged.

References

[1] J.E. Polk. *Cathode Erosion Mechanisms in Plasma Thrusters.* PhD thesis, Princeton University, Princeton, NJ, USA, To be published.

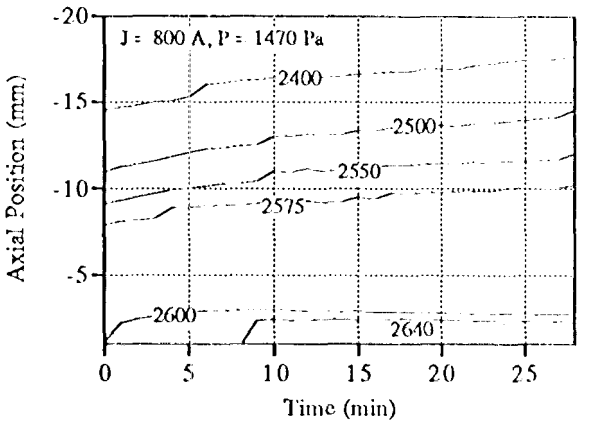

Figure *13:* Typical temperature contours.

[2] S. Anders and A. Anders. On Modes of Arc Cathode Operation. *IEEE Transactions on Plasma Science*, 19(1):20 24, 1991.

[3] K.D. Goodfellow and J.E. Polk. High Current Cathode Thermal Behavior, Part 1: Theory. In 23rd *International Electric Propulsion Conference*, Seattle, WA, 1993. AI AA-93030.

[4] R.M. Myers, N. Suzuki, A.J. Kelly, and R.G. Jahn. Cathode Phenomena in a Low Power, Steady MPD Thruster. In 24th *Joint Propulsion Conference*, Boston, MA, 1988. AI AA-88-3206.

[5] F.R. Chamberlain, A.J. Kelly, and R.G. Jahn. Electropositive Surface Layer MPD Thruster Cathodes. In 25th *Joint Propulsion Conference*, Monterey, CA, 1989. AIAA 89-2706.

[6] J.E. **I'elk,** A.J. Kelly, and R.G. Jahn. Mechanisms of Hot Catl iode Erosion in MPD Thrusters. In 21st *International Electric Propulsion Conference*, Orlando, FL, 19(JO. AlAA-90-2673.

[7] R. G. Jahn J. Fillmore, A. J. Kelly. Electric Propulsion Laboratory Progress Report. Technical Report 1776.42, Department of Mechanical and Aerospace Engineering, Princeton University, Princeton, NJ 08544, March/April 1993.

[8] W.L. Bade and J.M. Yes. A Theoretical and Experimental Study of Thermionic Arc Cathodes. Technical Report A SC-TDR-62-729, Air Force Materials Laboratory, Wright-Patterson A FB, 011, 1963.

[9] D.Q. King. Feasibility of Steady-State, Multi-Megawatt MPD Thrusters. In 18th *International Electric Propulsion Conference*, Alexandria, VA, 1985. AIAA-85-2004.

[10] G. Krülle. Zur Phänomenologie von Plasmatriebwerks Kathoden im Druckbereich zwischen 15 und 100 Torr. Technical Report DLR FB 66-26, Deutsche Versuchsanstalt fiir Luft- und Raumfahrt, April 1966.

[11] H. Hügel and G. Krülle. Phänomenologie und Energiebilanz von Lichtbogenkatoden bei niedrigen Drücken und hohen Stromstärken. *Beiträge aus der Plasma Physik*, 9(2):87- 116, 1969.

[12] R.M. Pon and J .1'. Hessler. Spectral Emissivity of Tungsten: Analytic Expressions for the 340-nm to 2600- nm Spectral Region. *Applied Optics*, 23:975 976, 1984.

[13] J .C. DeVos. A New Determination of the Emissivity of Tungsten Ribbon. *Physica*, 20:690 714, 1954.

[14] A.I. Funai and R.E. Rolling. Inspection Techniques for the Characterization of Smooth, Rough, and Oxide Surfaces. in G.B. Heller, editor, *Progress in Aeronautics and Astronautics. 1967.*

[15] O. Loesener, University of Stuttgart, Personal communication, May 1990.

[16] 11. Hügel. Vorgänge an Lichtbogenkathoden in strömenden Gasen bei niedrigen Drücken. *Astronautica Acta*, 11(4):247-251, 1965.

[17] M. Auweter-Kurtz, H. Kurtz, W. Merke, O. Loesener, I I, Schrade, T. Wegmann, D. Willer, and J. Polk. Cathode Phenomena in Plasma Thrusters. In 21st *International Electric Propu - sion Conference*, Orlando, FL, 1990. AI AA-90-2662.